

# Theory of Low-Temperature Hall Effect in Stripe-Ordered Cuprates

Jie Lin and A. J. Millis

*Department of Physics, Columbia University,*

*538 West 120th Street, New York, NY 10027*

## Abstract

We investigate the effect of static anti-phase stripe order on the weak-field Hall effect of electrons on a two-dimensional square lattice with electron dispersion appropriate to the high  $T_c$  cuprates. We first consider the cases where the magnitudes of the spin and charge stripe potentials are smaller than or of the same order as the bandwidth of the two-dimensional electrons, so that the electronic properties are not too strongly one-dimensional. In a model with only spin stripe potential, and at carrier concentrations appropriate to hole-doped cuprates, increasing the stripe scattering potential from zero leads to an increase in  $R_H$ , followed by a sign change. If the scattering amplitude is yet further increased, a second sign change occurs. The results are in semiquantitative agreement with data. In a charge-stripe-potential-only model,  $R_H$  increases as the charge stripe scattering strength increases, with no sign change occurring. In a model with both spin and charge stripe potentials,  $R_H$  may be enhanced or may change sign, depending on the strengths of the two scattering potentials. We also consider the case in which the magnitudes of the stripe potentials are much larger than the bandwidth, where analytical results can be obtained. In this limit, the system is quasi-one-dimensional, while  $R_H$  remains finite and its sign is determined by the carrier density and the electron band parameters.

PACS numbers: 74.72.Dn, 71.45.Lr, 75.47.Pq

## I. INTRODUCTION

Stripe order, static or fluctuating, is argued to be an important ingredient in understanding the physics of the high temperature superconductors.<sup>1,2</sup> In the  $\text{YBa}_2\text{Cu}_3\text{O}_{6+x}$  family, stripe order was recently used to explain<sup>3</sup> the small electron pockets observed in the quantum oscillation measurements.<sup>4,5</sup> In the family of materials derived from  $\text{La}_2\text{CuO}_4$ , stripe order is believed to be prevalent, being related to the “1/8 anomaly” observed in most members of this material family.<sup>6</sup> In the  $\text{La}_{1.6-x}\text{Nd}_{0.4}\text{Sr}_x\text{CuO}_4$  (Nd-LSCO) series, static stripe order has been shown by neutron diffraction measurements to exist over a significant part of the temperature–doping phase diagram,<sup>7</sup> up to Sr doping  $x \approx 0.25$ .

The Hall resistance of  $\text{La}_{1.6-x}\text{Nd}_{0.4}\text{Sr}_x\text{CuO}_4$  systems has been studied experimentally.<sup>8,9</sup> It was found that at the nominal hole doping  $x = 0.24$ , the low temperature Hall coefficient  $R_H$  takes the value appropriate to a two–dimensional metal with carrier (hole) density  $1 + x$ . However, for the lower dopings  $x = 0.20$  and  $x = 0.12$ , the measured  $R_H$  deviates significantly from what is expected for a conventional metal with carrier density  $1 + x$ . At  $x = 0.20$ ,  $R_H$ , while positive, is much larger than the value expected from the conventional model. For  $x = 0.12$ , the sign of  $R_H$  is opposite, showing an electron–like behavior. A similar issue arises in the electron–doped cuprates  $\text{Pr}_{2-x}\text{Ce}_x\text{CuO}_4$  (PCCO),<sup>10</sup> where the Hall number is positive for doping  $x > 0.15$  and becomes negative for smaller dopings. In the electron–doped material, the change of sign was explained by a commensurate  $(\pi, \pi)$  spin density wave order.<sup>11</sup> However, in the hole–doped materials,  $(\pi, \pi)$ –ordering would not produce a sign change. In this paper, we investigate whether stripe order can account for the magnitude and the unconventional doping dependence of the Hall resistivity observed in the La/Nd-Sr-Cu-O compounds.

The rest of this paper is organized as follows. Sec. II defines a phenomenological model for band electrons in the presence of stripe order, and summarizes the formulae used to calculate the conductivities. Sec. III illustrates the evolution of the Fermi surface in the stripe ordered state. Sec. IV discusses the effects of the charge stripe potential and the spin stripe potential on transport properties. Sec. V presents the doping dependence of  $R_H$  in the spin stripe ordered state. Sec. VI discusses the Hall effect in the strong stripe potential limit. Sec. VII is a conclusion in which the results are summarized and discussed and implications are outlined.

## II. MODEL AND FORMALISM

We assume electrons moving on a two-dimensional square lattice of unit lattice constant, with a band dispersion given by

$$\begin{aligned} \varepsilon_p = & -2t(\cos p_x + \cos p_y) + 4t' \cos p_x \cos p_y \\ & - 2t''(\cos 2p_x + \cos 2p_y). \end{aligned} \quad (1)$$

In our numerical calculations, we use the canonical values<sup>12</sup>  $t = 0.38\text{eV}$ ,  $t' = 0.32t$ , and  $t'' = 0.5t'$ . In addition, we assume that the electrons feel the effect of static “stripe” (spin and charge density wave) order. Because we are interested only in low-temperature transport, we neglect fluctuations and treat the order in the mean-field approximation.

We take the spin modulation to be longitudinal and to be described by the wave vector  $\mathbf{Q}_s$ , so that it gives rise to the scattering potential

$$\Delta_s(\mathbf{R}) = 2V \cos \mathbf{Q}_s \cdot \mathbf{R}.$$

The spatial periodicity of this potential can be obtained from the incommensurate peaks in neutron diffraction measurements. Tranquada *et.al.*<sup>13</sup> showed that in the Nd-LSCO series for  $x \lesssim 1/8$ ,  $\mathbf{Q}_s = \pi(1 - 2x, 1)$ , while for  $x > 1/8$ , the spin incommensurability is approximately doping independent, with wave vector  $\mathbf{Q}_s^* \approx \pi(3/4, 1)$ . We will be mainly interested in doping  $x > 1/8$ , so we fix  $\mathbf{Q}_s = \mathbf{Q}_s^*$ .

Charge modulations are also observed in the Nd-LSCO materials.<sup>14</sup> These occurs at the wave vector  $\mathbf{Q}_c = 2\mathbf{Q}_s$  expected from general Landau theory arguments, which allow a term  $S_Q^2 \rho_{-2Q}$  in the free energy, where  $S_Q$  and  $\rho_{-2Q}$  are the spin stripe and charge stripe order parameters, respectively.<sup>15</sup> We model the effect of charge stripes by the potential,

$$\Delta_Q(\mathbf{R}) = 2V_c \cos \mathbf{Q}_c \cdot \mathbf{R},$$

and we set  $\mathbf{Q}_c = 2\mathbf{Q}_s^* = \pi(1/2, 0)$ . We have approximated the stripe potentials as simple cosines; deviations from this form were investigated and found not to be important.<sup>3</sup>

These considerations lead to the following Hamiltonian:

$$H = \begin{pmatrix} \varepsilon_p & V_c & 0 & V_c & 0 & V & V & 0 \\ V_c & \varepsilon_{p+(\frac{1}{2},0)\pi} & V_c & 0 & 0 & 0 & V & V \\ 0 & V_c & \varepsilon_{p+(1,0)\pi} & V_c & V & 0 & 0 & V \\ V_c & 0 & V_c & \varepsilon_{p+(\frac{3}{2},0)\pi} & V & V & 0 & 0 \\ 0 & 0 & V & V & \varepsilon_{p+(\frac{1}{4},1)\pi} & V_c & 0 & V_c \\ V & 0 & 0 & V & V_c & \varepsilon_{p+(\frac{3}{4},1)\pi} & V_c & 0 \\ V & V & 0 & 0 & 0 & V_c & \varepsilon_{p+(\frac{5}{4},1)\pi} & V_c \\ 0 & V & V & 0 & V_c & 0 & V_c & \varepsilon_{p+(\frac{7}{4},1)\pi} \end{pmatrix}. \quad (2)$$

We assume that the low temperature DC transport can be described by the Boltzmann equation. We further assume, as is appropriate for low temperatures, that the relaxation is mainly due to randomly distributed impurities with a low density, leading to a constant scattering rate,  $1/2\tau$ . The expressions for the longitudinal and Hall conductivities then follow from solving the Boltzmann equation with the relaxation time approximation (for a detailed derivation, see Ref. [11]). Assuming the  $T \rightarrow 0$  limit can be taken, these expressions are one-dimensional integrals along the Fermi surface,

$$\sigma_{xx} = \frac{\sigma_Q}{4\pi^2} \tau \oint ds \frac{v_x(s)^2}{v_F(s)}, \quad (3)$$

$$\sigma_{yy} = \frac{\sigma_Q}{4\pi^2} \tau \oint ds \frac{v_y(s)^2}{v_F(s)}, \quad (4)$$

$$\sigma_{xy} = \sigma_Q \frac{B}{\Phi_0} \frac{1}{4\pi} \tau^2 \oint \mathbf{v} \times d\mathbf{v} \cdot \hat{\mathbf{z}}, \quad (5)$$

where  $s$  is the arc length coordinate along the 2D Fermi surface,  $\hat{\mathbf{z}}$  is the unit vector along the  $c$ -axis, and  $\mathbf{v}$  is the Fermi velocity. In these equations,  $\sigma_Q = e^2/\hbar$  is the conductance quantum, and  $\Phi_0 = hc/2e$  is the superconducting flux quantum. The Hall coefficient  $R_H = \sigma_{xy}/(B\sigma_{xx}\sigma_{yy}) = 1/nec$  with  $n$  an effective electron density per unit cell per plane.

We evaluate these equations by first identifying the bands which produce Fermi surface segments, then using a numerical search procedure to locate the Fermi surface. Typically,  $\sim 10^4$  Fermi surface points are used. We then compute the velocities at each point and evaluate the integrals by the trapezoidal rule.

### III. FERMI SURFACE EVOLUTION IN THE SPIN AND CHARGE STRIPE ORDERED STATES

As shown in Ref. [3], in the mean-field stripe ordered state the electron Fermi surface is reconstructed from the one obtained in the band theory calculation in a complicated way. The normal state Fermi surface for doping  $x = 1/8$  is shown as the solid line in Fig. [1], along with its translations by  $\mathbf{Q}_s = \pi(\frac{3}{4}, 1)$  (dashed line) and by  $(2\pi, 2\pi) - \mathbf{Q}_s = \pi(\frac{5}{4}, 1)$  (dashed-dotted line). For small  $V$  and/or  $V_c$ , reconstruction happens in the vicinity of the hot spots (shown as solid points in Fig. [1]), where the Fermi surface crosses itself upon translation by the stripe wave vectors. In Fig. [1], we only show two values of the stripe wave vectors for simplicity. The complete Fermi surface crossing can be found in Ref. [3].

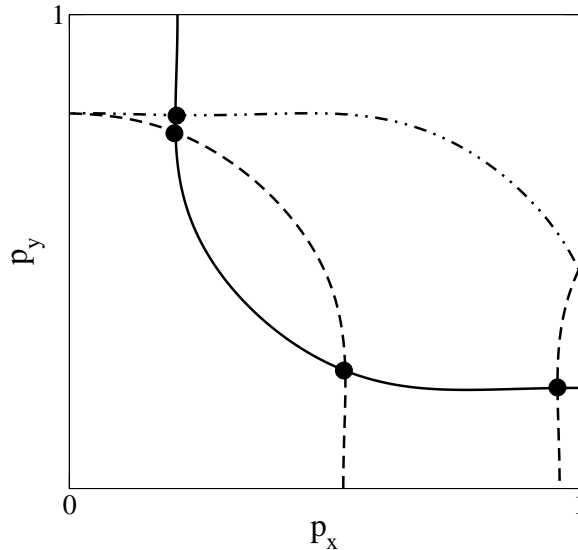


FIG. 1: The normal state Fermi surface (solid line) for doping  $x = 1/8$  and its translations by  $\mathbf{Q}_s = \pi(3/4, 1)$  (dashed line) and by  $(2\pi, 2\pi) - \mathbf{Q}_s = \pi(5/4, 1)$  (dashed-dotted line) in the first quadrant of the first Brillouin zone. The 4 hot spots are shown here as solid points. In this and the following Fermi surface plots, the unit of momentum  $p$  is  $\pi/a$ , with  $a = 1$  the lattice constant of the square lattice.

The Fermi surface evolution in the absence of the charge stripe potential is illustrated in Fig. [2], where the Fermi surfaces are plotted from left to right for increasing values of  $V$ . We see from Fig. [2(a)] that at relatively small  $V$ , there are well-defined hole pockets centered at  $(\pm\pi/8, \pi/2)$ , electron pocket centered at  $(0, \pi)$  and open Fermi surface. When

$V$  is increased further, the hole pockets are eliminated, Fig. [2(b)], and at a still larger  $V$ , the electron pocket is eliminated, leaving the open Fermi surface alone, Fig. [2(c)].

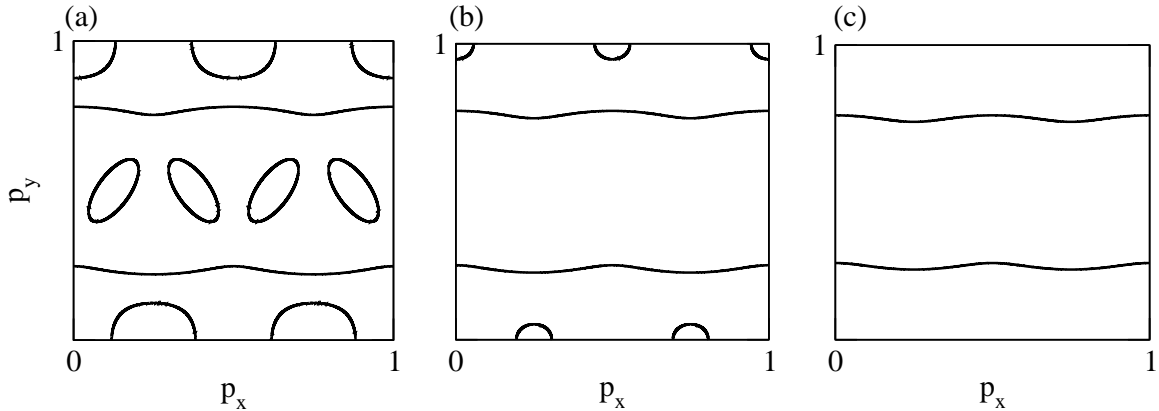


FIG. 2: Fermi surface evolution in the spin stripe ordered state, with the charge stripe potential  $V_c = 0$  and doping  $x = 1/8$ . (a):  $V = 0.2\text{eV}$ . (b):  $V = 0.25\text{eV}$ . (c):  $V = 0.3\text{eV}$ .

The Fermi surface evolution due to a charge stripe potential in the absence of the spin stripe potential is plotted in Fig. [3]. We see that for the two  $V_c$  values shown here, the Fermi surface is open, with no pockets.

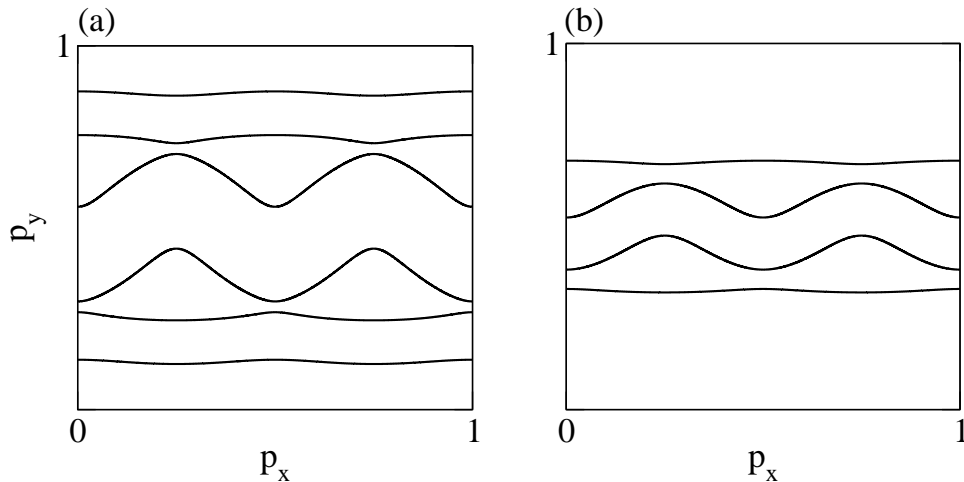


FIG. 3: Fermi surface in the charge stripe ordered state, with the spin stripe potential  $V = 0$  and a fixed doping  $x = 1/8$ . (a):  $V_c = 0.15\text{eV}$ . (b):  $V_c = 0.35\text{eV}$ .

When both types of stripe potentials are present, the Fermi surface reconstruction is more complicated. One representative Fermi surface is shown in Fig. [4]. In the case plotted, three bands cross the Fermi level. Two of them give open Fermi surfaces, while the third

one gives an electron pocket centered at  $(0, 0)$ .

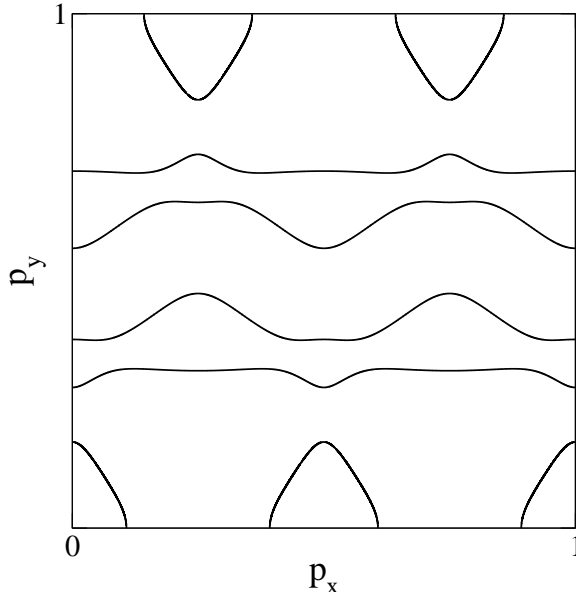


FIG. 4: The Fermi surface in the presence of both spin and charge stripe orders at doping  $x = 1/8$ ,  $V = 0.2\text{eV}$  and  $V_c = 0.3\text{eV}$ .

The consecutive changes of the Fermi surface topology upon changing the stripe potentials influence the Hall conductivity  $\sigma_{xy}$ , and the longitudinal conductivities  $\sigma_{xx}$  and  $\sigma_{yy}$ , and will be studied in the next section.

#### IV. HALL EFFECT: SPIN STRIPE POTENTIAL VS. CHARGE STRIPE POTENTIAL

##### A. Overview

In this section, we will consider the Hall effect in the spin and/or charge stripe potentials. Separate subsections treat different cases. We shall first consider the case where both potentials are weak, that is, the system is close to the quantum critical point from the normal state to the stripe ordered state. Then, we consider the cases of spin stripe potential only and charge stripe potential only, and finally the effects of combined spin- and charge- stripe scattering. In this section, we shall fix the doping to be  $x = 0.125$ , where the stripe order is most stable, and study the Hall effect, changing the strength of the stripe potentials  $V$  and  $V_c$ . In section V, we treat the doping dependence.

## B. Critical Behavior close to the Stripe Order Quantum Phase Transition

At small  $V$  and/or  $V_c$ , the Fermi surface reconstructs in the vicinity of the hot spots; it is essentially unchanged far from those points. Thus, although there are several Fermi surface crossings due to the  $8 \times 8$  matrix structure of  $H$ , the total changes in  $\sigma_{xy}$ ,  $\sigma_{xx}$  and  $\sigma_{yy}$  are additive. For each Fermi surface crossing, our previous analysis<sup>11</sup> applies. We find  $\delta\sigma_{xy}$  and  $\delta\sigma_{xx} + \delta\sigma_{yy}$  are both linear in  $V$  and  $V_c$ , such that as  $V \rightarrow 0$  and  $V_c \rightarrow 0$ ,

$$\frac{\delta R_H}{R_H^0} = \frac{\delta\sigma_{xy}}{\sigma_{xy}^0} - \frac{\delta\sigma_{xx} + \delta\sigma_{yy}}{\sigma_{xx}^0} = aV + bV_c, \quad (6)$$

where the superscript 0 denotes the corresponding value in the normal state, and we have used the fact that the normal state has 4-fold symmetry, so that  $\sigma_{xx}^0 = \sigma_{yy}^0$ . The prefactors  $a$  and  $b$  can be determined;  $a \approx 6\text{eV}^{-1}$ , and  $b \approx 10\text{eV}^{-1}$ . In the case of PCCO,<sup>11</sup> this asymptotic formula holds only within 1% of the critical value. The more complicated Fermi surfaces found here will restrict the domain of validity even further. For the very small values of  $V$  and  $V_c$  for which Eq. [6] applies, there are complications due to strong field crossover<sup>16</sup> or magnetic breakdown.<sup>17</sup>

## C. Spin Stripe Potential Only

In this subsection, we consider the case where the electrons are scattered only from the spin stripe potential, namely,  $V_c = 0$ . For each value of  $V$ , we calculate the loci of the Fermi surface and the Fermi velocities, and use this information in Eqs. [3–5]. Fig. [5] shows the results of such a calculation. We note that the onset of the stripe potential suppresses both the longitudinal and the Hall conductivities, Fig. [5(a)–(c)], as in the case of the commensurate spin density wave order in PCCO.<sup>11</sup> Fig. [2] shows the corresponding Fermi surfaces for the three nonzero  $V$  values. We can see that the behavior of  $\sigma_{xy}$  can be qualitatively understood in terms of the evolution of the Fermi surface topology.<sup>18</sup> For  $V = 0.2\text{eV}$ ,  $R_H$  is positive and significantly larger than the value in the normal state. The sign is due to the dominant hole pockets (Fig. [2(a)]), and the enhancement is due to the strong decrease of the longitudinal conductivities. When  $V$  grows large enough (0.25eV here),  $R_H$  becomes negative. This reversal of sign comes from the elimination of the hole pockets (Fig. [2(b)]). The smallness of the open Fermi surface contribution to  $\sigma_{xy}$  means that the electron pocket determines the sign of  $R_H$ . At still larger  $V$  (0.3eV), the electron



pocket is eliminated (Fig. [2(c)]). The open Fermi surface gives rise to a small positive contribution to  $\sigma_{xy}$  (hole-like), so  $R_H$  becomes positive again. However, the sign of  $R_H$  due to the open Fermi surface changes as  $V$  is increase further. As will be shown in Sec. VI, the crossover to the strong coupling limit occurs at  $V \sim 1\text{eV}$ .

We notice that in the cases with  $V = 0.25\text{eV}$  and  $0.3\text{eV}$ ,  $|R_H|$  is quite large compared to the band value  $R_H(V = 0)$ , although  $\sigma_{xy}$  is much smaller than  $\sigma_{xy}(V = 0)$ . This is due to the large anisotropy, as measured by  $\sigma_{yy}/\sigma_{xx}$ , for these two  $V$  values. This anisotropy is due to the open Fermi surfaces and grows rapidly with increasing  $V$ . This anisotropy compensates for the smallness of  $\sigma_{xy}$ , giving a large  $R_H$ .

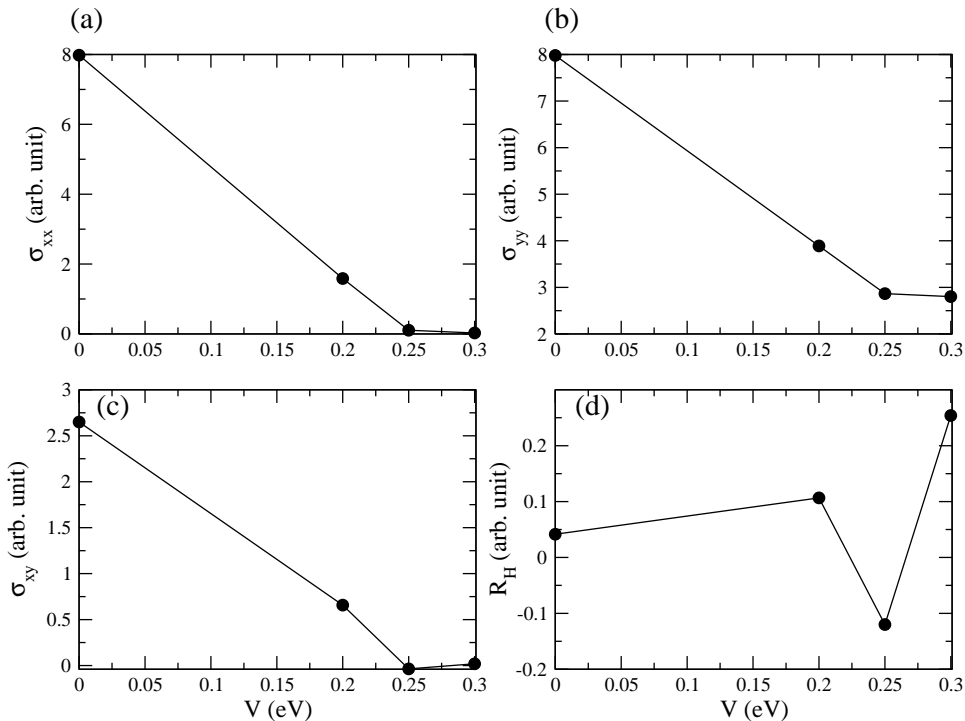


FIG. 5: Transport coefficients in the spin stripe ordered state at doping  $x = 1/8$  and  $V_c = 0$ . (a):  $\sigma_{xx}$  as a function of  $V$ . (b):  $\sigma_{yy}$  as a function of  $V$ . (c):  $\sigma_{xy}$  as a function of  $V$ . (d):  $R_H$  as a function of  $V$ . Here and in the following plots of the transport properties, the solid lines are guides to the eye; exceptions will be stated explicitly.

Fig. [5(d)] shows  $R_H$  for the 3 values of  $V$ . We see that as  $V$  grows,  $R_H$  first increases such that at  $V = 0.2\text{eV}$ ,  $R_H/R_H^0 \approx 2.5$ , and then decreases to a negative value. This trend is qualitatively consistent with the experimental data. In the next section, we shall study the doping dependence of  $R_H$ , assuming a model in which the spin stripe potential

opens at  $x = 0.24$  and grows as doping is reduced. We shall see that such a model can semi-quantitatively account for the experimental data.

#### D. Charge Stripe Potential Only

We now consider the effects of  $V_c$  on the transport properties with the spin potential set to 0, Fig. [6]. Fig. [3] shows 2 representative Fermi surfaces for  $V_c = 0.15\text{eV}$  and  $V_c = 0.35\text{eV}$ . For  $V_c$  in this range, all the pieces of the Fermi surface are open. However, some pieces of the open Fermi surface have relatively large curvature, because they can be viewed as the merging of the hole Fermi pockets. As shown in Fig. [6(c)],  $\sigma_{xy}$  is thus always relatively large even for  $V_c = 0.35\text{eV}$ . From Fig. [6(d)], we see that the onset of the charge stripe order gives a rapid increase of  $R_H$ . In fact,  $R_H(V = 0, V_c = 0.2\text{eV}) = 1.5R_H(V = 0.2\text{eV}, V_c = 0)$ . We also notice that the anisotropy is less than that in the spin stripe case; in the spin stripe case,  $\sigma_{yy}/\sigma_{xx} \approx 100$  at  $V = 0.3\text{eV}$ , while in the charge stripe case,  $\sigma_{yy}/\sigma_{xx} \approx 15$  at  $V_c = 0.35\text{eV}$ .

We see that although the increase of the charge stripe potential substantially enhances  $R_H$ ,  $R_H$  remains positive for all the four  $V_c$  values considered here. Further calculation (not shown here) suggests that  $R_H$  changes sign around  $V_c = 0.8\text{eV}$ , and approaches a negative value in the limit  $V_c \gg t$ . This suggests that a model with only charge stripe order is inconsistent with experimental data.

#### E. Coexistence of the Spin Stripe Potential and the Charge Stripe Potential

Now we study the case in which the spin stripe and the charge stripe coexist,  $V \neq 0$  and  $V_c \neq 0$ . The interplay between these two stripe potentials leads to very complicated behavior of  $R_H$ . Fig. [7] shows two representative sets of results. In both cases, we fix  $V$  and increase  $V_c$  from 0 to a large value. Fig. [7(a)] shows  $R_H(V_c)$  for  $V = 0.2\text{eV}$ . In this case,  $R_H(V_c = 0) > 0$ , and at a small  $V_c = 0.05\text{eV}$ ,  $R_H$  is strongly enhanced by a factor of 1.5. For  $V_c = 0.3\text{eV}$ ,  $R_H$  becomes negative, while at larger  $V_c$ ,  $R_H$  is positive again. Fig. [7(b)] shows  $R_H$  as a function of  $V_c$  for  $V = 0.25\text{eV}$ . In this case,  $R_H(V_c = 0) < 0$ . At a small value of  $V_c = 0.05\text{eV}$ , the sign is reversed to be hole-like, while at larger  $V_c$ ,  $R_H$  becomes negative again.

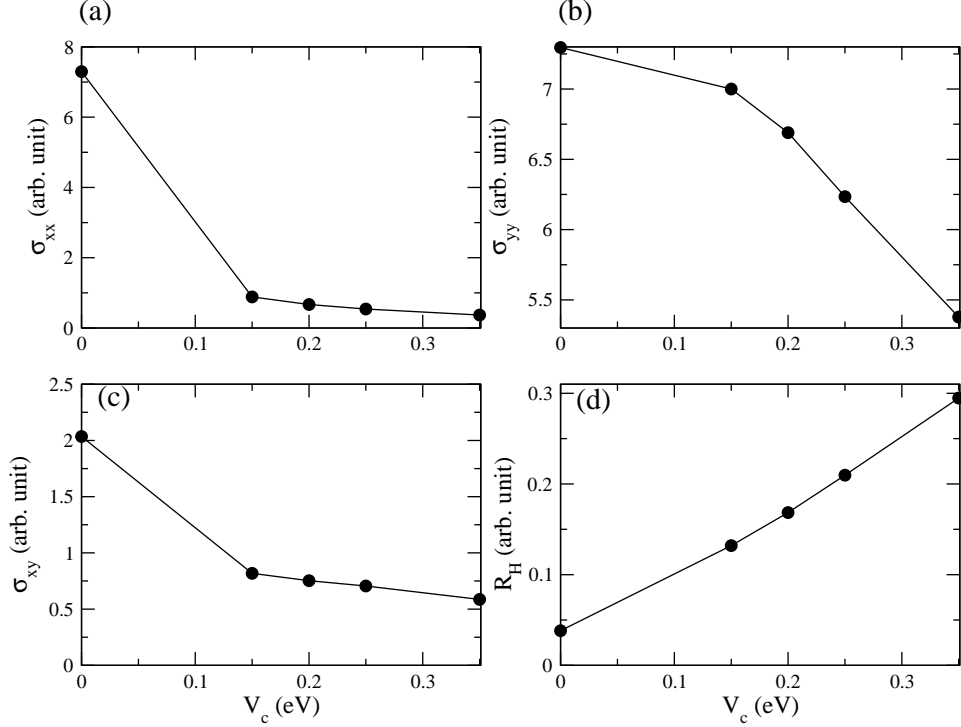


FIG. 6: Transport coefficients in the charge stripe ordered state calculated for doping  $x = 1/8$  and  $V = 0$ . (a):  $\sigma_{xx}$  as a function of  $V_c$ . (b):  $\sigma_{yy}$  as a function of  $V_c$ . (c):  $\sigma_{xy}$  as a function of  $V_c$ . (d):  $R_H$  as a function of  $V_c$ .

The behavior of  $R_H$  can be understood in terms of the evolution of the Fermi surface topology when changing  $V_c$  and  $V$ . In the case of  $V = 0.2\text{eV}$ , for both  $V_c = 0.05\text{eV}$  and  $V_c = 0.1\text{eV}$ , the calculated Fermi surface (not shown) closely resembles that in Fig. [2(a)], explaining the positive sign of  $R_H$ . For the case  $V_c = 0.3\text{eV}$ , the Fermi surface is given in Fig. [4] and has a qualitatively different topology, such that the hole Fermi surface becomes open, and the electron pocket (which now dominates  $\sigma_{xy}$ ) changes from being centered at  $(0, \pi)$  to being centered at  $(0, 0)$ . At larger values of  $V_c$ , the electron pocket is eliminated, leaving open Fermi surface only, qualitatively resembling Fig. [3(b)]. The sign of  $\sigma_{xy}$  is calculated to be positive.

In the case of stronger  $V = 0.25\text{eV}$ , the  $V_c = 0$  Fermi surface is shown in Fig. [2(b)]. At  $V_c = 0.05\text{eV}$ , the hole pockets reappear, with a very small radius, leading to a Fermi surface very similar to that in Fig. [2(a)]. However, the small hole pockets dominate the sign of  $R_H$ . The hole Fermi pockets grow with increasing  $V_c$ , and eventually merge into open Fermi surface at large  $V_c$ . For  $V_c = 0.3\text{eV}$ , the Fermi surface topology changes qualitatively as

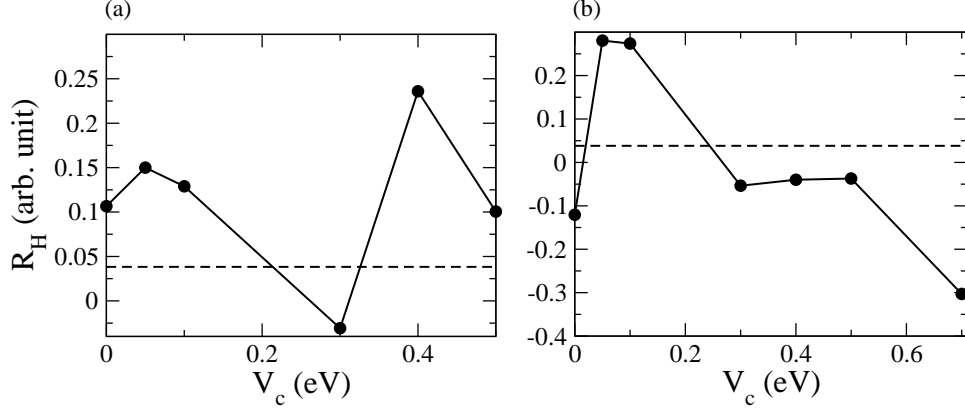


FIG. 7:  $R_H$  for nonzero  $V$  and nonzero  $V_c$  and doping  $x = 1/8$ . (a):  $V = 0.2\text{eV}$ ; (b):  $V = 0.25\text{eV}$ . Dashed line indicates the position of  $R_H^0$ .

in the case of  $V = 0.2\text{eV}$  and  $V_c = 0.3\text{eV}$ , Fig. [4]. This Fermi surface reconstruction can qualitatively explain the negative sign of  $R_H$  at  $V_c = 0.3\text{ eV}$ . At  $V_c = 0.5\text{ eV}$  and  $0.7\text{ eV}$ , the electron pocket is eliminated, leaving only open Fermi surface, as qualitatively represented in Fig. [3(b)]. However, the sign of  $R_H$  remains negative.

The discussion in this section shows that the interplay between the spin and the charge stripe potentials leads to two possibilities to account for the experimental observation of the sign change of  $R_H$ . In the simplest case, the spin stripe order is dominant, and the charge stripe order potential is small;  $V_c$  should be less than  $0.05\text{eV}$  when  $V = 0.25\text{eV}$  and  $x = 1/8$ . Then we assume that  $V_c$  can be neglected. In the other scenario, both  $V$  and  $V_c$  are large, as shown in Fig. [7]. In the next section, we pursue the first scenario in more detail.

## V. HALL EFFECT: DOPING DEPENDENCE

We now study the doping dependence of the transport coefficients. Doping has two effects, changing the carrier density and changing the strength of the stripe potential. From the discussion of the last section, we assume a model for the electrons in the stripe ordered state in which the spin stripe scattering is dominant, and the charge stripe scattering is neglected.

We assume a mean field dependence of the stripe order parameter on doping, for  $x < 0.24$

$$V = V_0 \sqrt{1 - x/0.24}, \quad (7)$$

and  $V = 0$  for  $x > 0.24$ , where  $V_0$  controls the rate at which the stripe order is setting in. Experimental results show that the  $x = 0.12$  sample has a negative  $R_H$ . Fig. [5(d)] suggests that  $V_0$  should be relatively large, such that  $0.2 < V(x = 0.12) < 0.3\text{eV}$ . Thus, we choose  $V_0 = 0.35\text{eV}$ . Then for each doping  $x$ , the conductivities and the Hall coefficient can be calculated from Eqs. [3–5]. The results are shown in Fig. [8]. We observe that  $R_H$  starts at  $x = 0.24$  ( $V = 0$ ) at the band value  $1/(1+x)$ , increases as doping is decreased, and jumps to a negative number around  $x = 0.13$ .

In terms of the Fermi surface evolution, for doping  $x = 0.12$ , the Fermi surface can be represented by Fig. [2(b)], for doping  $x = 0.125$ , the Fermi surface resembles that in Fig. [2(a)] with tiny hole pockets, and for doping in the range  $0.13 \leq x < 0.16$ , the Fermi surfaces can be represented by Fig. [2(a)].

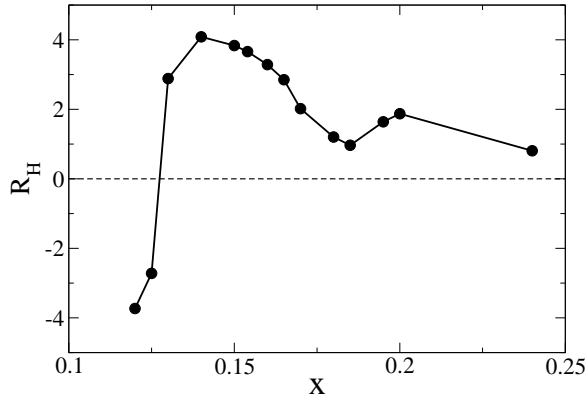


FIG. 8:  $R_H$ , expressed as the inverse of the effective carrier density per plane per cell, as a function of doping. The spin stripe potential  $V$  takes a mean field form  $V[\text{eV}] = 0.35\sqrt{1-x/0.24}$ , and the charge stripe potential is neglected,  $V_c = 0$ .  $R_H(x = 0.24) \approx 0.8 \approx 1/(1+x)$ . Dashed line indicates  $R_H = 0$ .

We see that  $R_H$  has a local minimum around  $x = 0.18$ . Starting from  $x = 0.15$ , and increasing doping (decreasing  $V$ ),  $R_H$  first decreases rapidly, and after  $x \approx 0.18$ , it increases, and then decreases again to the band value  $R_H^0$ . This can be qualitatively understood in terms of the Fermi surface evolution. At  $x = 0.15$ , the Fermi surface resembles that in Fig. [2(a)]. Increasing doping, the size of the hole pockets centered at  $(\pm\pi/8, \pi/2)$  increases. These hole pockets eventually merge into open Fermi surface, see Fig. [9(a)] for  $x = 0.18$ . Increasing  $x$  further, new pieces of Fermi surface appear, as shown in Fig. [9(b)], which are hole-like, and contribute to the increase of  $R_H$  around  $x = 0.2$ . Because the structure of

$R_H$  in the doping range  $0.15 < x < 0.2$  arises from the small pockets shown in Fig.[9(b)], we believe it will be very sensitive to details and extrinsic effects including scattering and magnetic breakdown. Increasing doping toward  $x = 0.24$  where  $V = 0$ ,  $R_H$  is then described by the critical behavior,  $\delta R_H/R_H^0 = aV$ , with positive  $a$ .

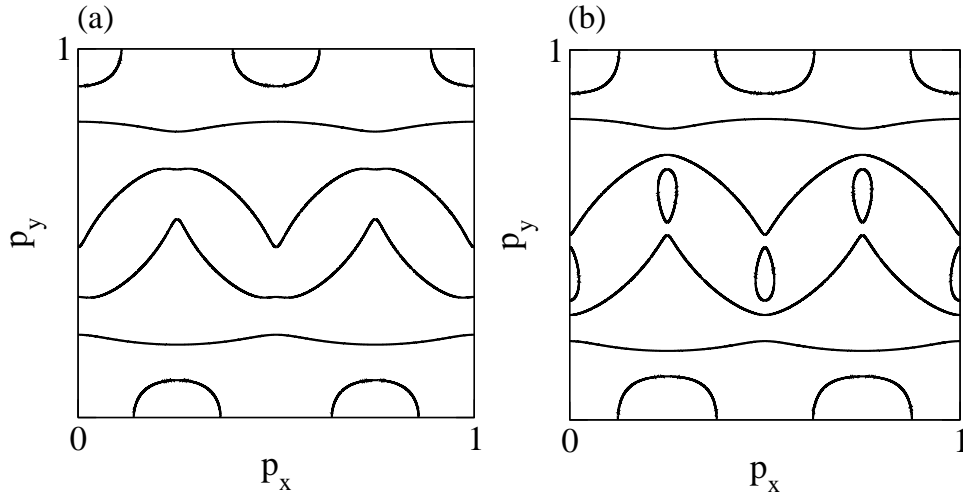


FIG. 9: Fermi surfaces for relatively small  $V$ . (a):  $V = 0.175\text{eV}$ ,  $V_c = 0$ , and doping  $x = 0.18$ . (b):  $V = 0.143\text{eV}$ ,  $V_c = 0$ , and doping  $x = 0.20$ .

## VI. LARGE STRIPE POTENTIAL LIMIT

In this section, we consider the case where the stripe potential  $V \gg t$  and the hole doping is in the range  $0.125 < x < 0.25$ . We assume that, on average, no two electrons occupy the same lattice site. We will see that this constraint requires that  $2V_c < V$ . Fig. [10(a)] shows the spin stripe potential for spin-up electrons. (The spin potential for spin-down electrons is opposite.)

For large spin potentials, the doped holes reside on the columns where  $\Delta_s = 0$  (the circles without arrows in Fig. [10(a)]), referred to as charge stripes. The doped holes mainly move along these charge stripes, with a small probability to hop from one stripe to another. A general Hamiltonian for charges moving in weakly coupled stripes of spacing 4 lattice constants is

$$H = \varepsilon^0(p_y) + \sum_n f_n(p_y) \cos 4np_x, \quad (8)$$

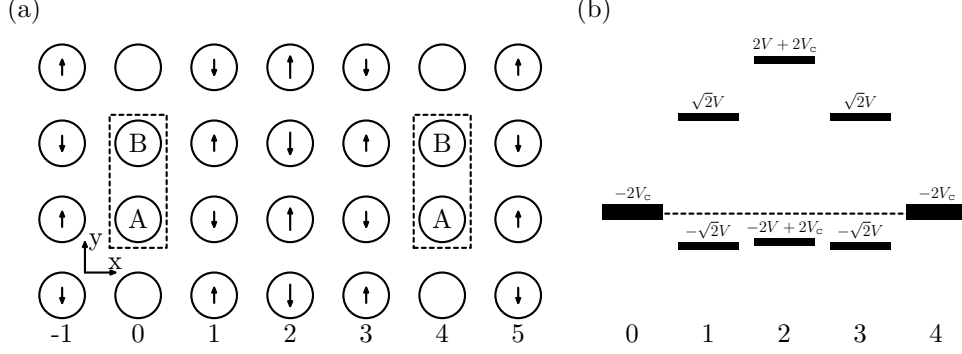


FIG. 10: (a): the spin stripe potential for spin-up electrons. For spin-down electrons, the arrows are opposite. The length of arrows is proportional to the magnitude of the potential. The charge stripe potential is not shown here. (b): the energy bands for each column represented by the filled boxes, with height proportional to the bandwidth. In this plot,  $V = 3V_c$  and hole doping  $x = 0.125$ . The Fermi level is shown as dashed line.

with small  $f_n$ . From Eq. [5], the Hall conductivity is

$$\sigma_{xy} = -\mathcal{A} \int_{-\pi}^{\pi} dp_x v^y(p_x) \frac{dv^x(p_x)}{dp_x}, \quad (9)$$

where  $\mathcal{A} = \sigma_Q \frac{B}{\Phi_0} \frac{1}{2\pi} \tau^2$ . At  $f_n = 0$ , the Fermi surface is  $p_y = p_0$ , and the dispersion may be approximated by

$$\varepsilon^0(p_0 + \delta p_y) = v_0 \delta p_y + \frac{1}{2} m_0 \delta p_y^2. \quad (10)$$

To leading order in  $f_n$ , we find

$$\sigma_{xy} = -16\pi \mathcal{A} \sum_n n^2 \left( \frac{m_0}{v_0} - \frac{1}{f_n} \frac{df_n}{dp_y} \right) f_n^2, \quad (11)$$

with all quantities evaluated at  $p_0$ . In most cases we find that the sign of the Hall effect is determined by the curvature of the 1D band ( $m_0/v_0$ ); but for some particular parameter values, structure in the interchain hopping can produce a sign change, for example, when one of the  $f_n$  goes through zero.

The longitudinal conductivities  $\sigma_{xx,yy}$  can be calculated in a similar manner in terms of  $f_n$ . To leading order in  $f_n$ , Eq. [3] can be approximated as

$$\sigma_{xx} = \mathcal{B} \int_{-\pi}^{\pi} dp_x \sqrt{1 + \left( \frac{dp_y}{dp_x} \right)^2} (v^x)^2 / \sqrt{(v^x)^2 + (v^y)^2} \approx \mathcal{B} \frac{16\pi}{|v_0|} \sum_n n^2 f_n^2 \quad (12)$$

where  $\mathcal{B} = \sigma_Q \tau / (4\pi^2)$  and  $f_n$  is evaluated at  $p_0$ . Eq. [4] can be approximated as

$$\sigma_{yy} \approx \mathcal{B} \int_{-\pi}^{\pi} dp_x |v_0| = \mathcal{B} 2\pi |v_0|. \quad (13)$$

In the rest of this section, we present an evaluation of  $f_n$  in the strong coupling limit using perturbation theory.

The zeroth order Hamiltonian describes the motion of electrons along the  $y$ -direction, as defined in Fig. [10(a)], in the stripe potential. The unit cell is doubled along this direction due to the spin potential, as shown by the boxes in Fig. [10(a)]. It is convenient to introduce a pseudo-spinor operator,

$$\hat{\psi}_{xy} = \begin{pmatrix} \psi_{xy}^B \\ \psi_{xy}^A \end{pmatrix}, \quad (14)$$

where  $y$  is now multiples of 2 lattice constants, and  $\psi_{xy}^{A,B}$  is the electron annihilation operator. Then, for the column  $x = n$ , the zeroth order Hamiltonian is given by

$$\mathcal{H}_n^{(0)} = \sum_{p_y} \hat{\psi}_{n,p_y}^\dagger \hat{H}_{n,p_y}^{(0)} \hat{\psi}_{n,p_y}, \quad (15)$$

with

$$\hat{H}_{n,p_y}^{(0)} = V_n^c + V_n^s \hat{\tau}_z - 2t'' \cos 2p_y - t[(1 + \cos 2p_y)\hat{\tau}_x - \sin 2p_y \hat{\tau}_y], \quad (16)$$

where  $\hat{\tau}$ 's are the Pauli matrices, and  $V_0^c = -V_2^c = -2V_c$ ,  $V_1^c = V_3^c = 0$ ,  $V_0^s = 0$ ,  $V_1^s = V_3^s = \sqrt{2}V$ , and  $V_2^s = -2V$ . After a canonical transformation  $\mathcal{T}$ , which rotates the pseudo-spinor  $\hat{\psi}$  in the pseudo-spin space first about the  $\hat{\tau}_z$ -axis by  $p_y/2$  and then about the  $\hat{\tau}_y$ -axis by  $\pi/2$ , Eq. [16] becomes

$$\hat{H}_{n,p_y}^{(0)} = V_n^c + V_n^s \hat{\tau}_x - 2t'' \cos 2p_y + 2t \cos p_y \hat{\tau}_z. \quad (17)$$

The energy bands on the column  $n = 0$  are

$$E_\pm^0 = -2V_c - 2t'' \cos 2p_y \pm 2t |\cos p_y|, \quad (18)$$

with corresponding wave functions

$$|+\rangle = \begin{pmatrix} \theta(\cos p_y) \\ \theta(-\cos p_y) \end{pmatrix}, \quad |-\rangle = \begin{pmatrix} \theta(-\cos p_y) \\ \theta(\cos p_y) \end{pmatrix}. \quad (19)$$

For hole doping  $x$  in the range  $0.125 < x < 0.25$ ,  $\varepsilon^0(p_y) = E_-^0$ . To leading order in  $t/V$ , the energy bands are  $E_\pm^1 = \pm\sqrt{2}V$  on the column  $n = 1$ ,  $E_\pm^2 = 2V_c \pm 2V$  on the column  $n = 2$ , and  $E_\pm^3 = \pm\sqrt{2}V$  on the column  $n = 3$ . Fig. [10(b)] shows these energy bands for each column.



The motion of electrons along the  $x$ -direction is described by

$$\mathcal{H}^X = \sum_{n,p_y} [\hat{\psi}_{n+1,p_y}^\dagger H_{p_y}^+ \hat{\psi}_{n,p_y} + h.c.] + \sum_{n,p_y} [\hat{\psi}_{n+2,p_y}^\dagger H^{++} \hat{\psi}_{n,p_y} + h.c.], \quad (20)$$

where, after the canonical transformation  $\mathcal{T}$ ,

$$H_{p_y}^+ = -t - 2t' \cos p_y \hat{\tau}_z, \quad (21)$$

and

$$H^{++} = -t''. \quad (22)$$

We calculate the matrix elements for electrons (holes) to hop from one charge stripe to a nearby stripe by perturbation theory using  $\mathcal{H}^X$  as a perturbation. In the following, we first consider the case where there is no charge potential, and then consider the case where the charge potential  $V_c$  is nonzero.

### A. Spin Stripe Potential Only

In the absence of the charge potential, the leading order terms in the matrix elements that describe electrons hopping among charge stripes are of order  $1/V^2$ . To this order, there are three possible processes, whose matrix elements are denoted by  $M^A$ ,  $M^B$  and  $M^C$ .  $M^A$  is given by

$$M^A = \langle - | H^{++} \frac{1}{E_-^0 - \hat{H}_{2,p_y}^{(0)}} H^{++} | - \rangle, \quad (23)$$

and represents the hopping between stripes  $n = 0$  and  $n = 4$  by two  $H^{++}$ .  $M^B$ , which represents the hopping between stripes  $n = 0$  and  $n = 4$  by two  $H_{p_y}^+$  and one  $H^{++}$ , is given by the sum of the three terms,

$$M_{211}^B = \langle - | H^{++} \frac{1}{E_-^0 - \hat{H}_{2,p_y}^{(0)}} H_{p_y}^+ \frac{1}{E_-^{(0)} - \hat{H}_{3,p_y}^{(0)}} H_{p_y}^+ | - \rangle, \quad (24)$$

$$M_{121}^B = \langle - | H_{p_y}^+ \frac{1}{E_-^0 - \hat{H}_{1,p_y}^{(0)}} H^{++} \frac{1}{E_-^{(0)} - \hat{H}_{3,p_y}^{(0)}} H_{p_y}^+ | - \rangle, \quad (25)$$

and

$$M_{112}^B = \langle - | H_{p_y}^+ \frac{1}{E_-^0 - \hat{H}_{1,p_y}^{(0)}} H_{p_y}^+ \frac{1}{E_-^0 - \hat{H}_{2,p_y}^{(0)}} H^{++} | - \rangle. \quad (26)$$

$M^C$  represents the hopping between stripes  $n = 0$  and  $n = 8$  by four  $H^{++}$ , and is given by

$$M^C = \langle -|H^{++} \frac{1}{E_-^0 - \hat{H}_{2,p_y}^{(0)}} H^{++}|+ \rangle \frac{1}{E_-^0 - E_+^0} \langle +|H^{++} \frac{1}{E_-^0 - \hat{H}_{6,p_y}^{(0)}} H^{++}| - \rangle, \quad (27)$$

where  $V_6^s = -V_2^s$ .

To order  $1/V^2$ , the Hamiltonian  $H$  in Eq. [8] is

$$H = \varepsilon^0(p_y) + f_1(p_y) \cos 4p_x + f_2(p_y) \cos 8p_x, \quad (28)$$

where

$$\begin{aligned} f_1 &= 2(M^A + M_{112}^B + M_{121}^B + M_{211}^B) \\ &= \frac{2tt''}{V^2} (2t' + t'') |\cos p_y| - \frac{t''}{V^2} [(1 - \sqrt{2})t^2 + 4(1 + \sqrt{2})t'^2 \cos^2 p_y], \end{aligned} \quad (29)$$

$$f_2 = 2M^C = -\frac{t''^4}{8tV^2 |\cos p_y|}, \quad (30)$$

and we have neglected the hopping processes in which an electron hops from a charge stripe into the region between stripes with a large potential and hops back to the same stripe. These processes give corrections to  $\varepsilon^0(p_y)$  of order  $1/V^2$  with no  $p_x$ -dependence, and thus have no effects on  $R_H$  to leading order. Eq. [28] can also be obtained from third order perturbation calculation of Eq. [2], treating  $\varepsilon_p$  as a perturbation.

Substituting Eqs. [29,30] into Eq. [11], we obtain the Hall conductivity  $\sigma_{xy}$  to leading order in  $1/V$  in the large- $V$  limit,

$$\sigma_{xy} = -\frac{16\pi\mathcal{A}}{V^4} \left\{ f_1^2 \left( \frac{m_0}{v_0} - \frac{1}{f_1} \frac{df_1}{dp_y} \right) + 4f_2^2 \left( \frac{m_0}{v_0} - \frac{1}{f_2} \frac{df_2}{dp_y} \right) \right\} \equiv \frac{1}{V^4} \mathcal{S}_{xy}, \quad (31)$$

where all the quantities are evaluated at  $p_0$  which is determined by the carrier density. Since both  $\sigma_{xx}$  and  $\sigma_{yy}$  are positive-definite, the sign of  $R_H$  is determined by that of  $\sigma_{xy}$ . Similarly, substituting  $f_1$  and  $f_2$  into Eqs. [12,13], we obtain the leading order terms of  $\sigma_{xx}$  and  $\sigma_{yy}$ ,

$$\sigma_{xx} = \frac{1}{V^4} \mathcal{B} \frac{16\pi}{|v_0|} (f_1(p_0)^2 + 4f_2(p_0)^2) \equiv \frac{1}{V^4} \mathcal{S}_{xx}, \quad (32)$$

and

$$\sigma_{yy} = \mathcal{B} 2\pi |v_0| \equiv \sigma_{yy}^\infty. \quad (33)$$

So  $R_H$  approaches a constant as the stripe potential  $V \rightarrow \infty$ ,

$$\lim_{V \rightarrow \infty} R_H = \frac{\mathcal{S}_{xy}}{\mathcal{S}_{xx} \sigma_{yy}^\infty} \equiv R_H^\infty. \quad (34)$$

We observe that  $\mathcal{S}_{xy}$ ,  $\mathcal{S}_{xx}$ ,  $\sigma_{yy}^\infty$  and  $R_H^\infty$  are determined by the carrier density and the band parameters  $t$ ,  $t'$ , and  $t''$ . We perform numerical calculations of the conductivities  $\sigma_{xx,xy,yy}$  and the Hall coefficient  $R_H$  for the spin stripe potential  $V$  up to 10eV, doping  $x = 0.125$ ,  $V_c = 0$ , and the canonical values of the band parameters:  $t = 0.38\text{eV}$ ,  $t' = 0.32t$ , and  $t'' = 0.5t'$ . The results are shown as dots in Fig. [11], where we compare these numerical results to the corresponding  $V \rightarrow \infty$  limits (solid lines). We observe that the numerical results indeed approach the expected values. There are small discrepancies, which we attribute to the errors in calculating the chemical potential and in numerically finding the Fermi surface. For the parameters used here,  $R_H^\infty < 0$ . In Sec. IV, we showed that for  $V = 0.3\text{eV}$ , there is only open Fermi surface and  $R_H > 0$ . Thus there is a change of sign in  $R_H$  for  $V > 0.3\text{eV}$  (roughly at  $V = 1\text{eV}$ , Fig. [11(d)]). This sign change can be understood qualitatively from Eqs. [8,11], where we argued that  $\sigma_{xy}$  changes sign when one of the  $f_n$  goes through zero. We compared the Fermi surfaces for  $V$  close to 1eV, and found strong evidence that at least one of the  $f_n$  in Eq. [8] changes sign.

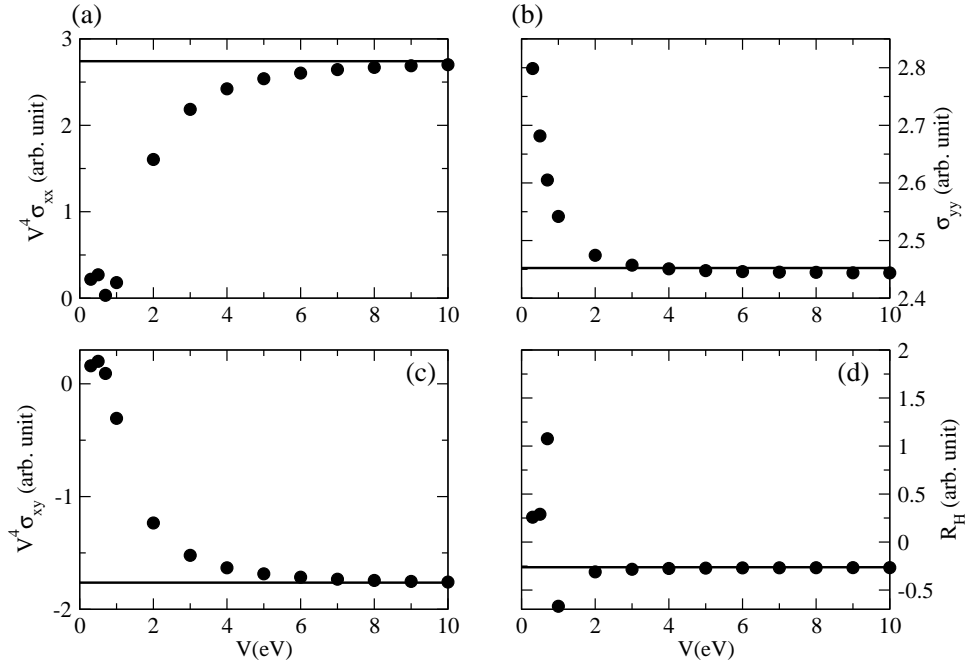


FIG. 11: Numerical results of the transport coefficients at large spin stripe potential  $V$ , for doping  $x = 0.125$ ,  $V_c = 0$ , and for the canonical values of  $t$ ,  $t'$ , and  $t''$ . (a):  $V^4 \sigma_{xx}$  (dots) and  $\mathcal{S}_{xx}$  (solid line). (b):  $\sigma_{yy}$  (dots) and  $\sigma_{yy}^\infty$  (solid line). (c):  $V^4 \sigma_{xy}$  (dots) and  $\mathcal{S}_{xy}$  (solid line). (d):  $R_H$  (dots) and  $R_H^\infty$  (solid line).

We now study the dependence of  $R_H^\infty$  on doping and band parameters. Fig. [12] shows  $R_H^\infty$  as a function of doping, using the canonical values of the band parameters:  $t'/t = 0.32$  and  $t''/t = 0.16$ . We also calculated  $R_H$  as a function of doping numerically for  $V = 10\text{eV}$ , shown as dots in Fig. [12]. There is a good agreement between the numerical results and  $R_H^\infty$ . We observe that for the canonical values of the band parameters and in the doping range  $0.125 < x < 0.25$ ,  $R_H^\infty < 0$ . The sign of  $R_H^\infty$  as a function of the band parameters  $t'/t$  and  $t''/t$  for doping  $x = 0.125$  is plotted in Fig. [13], which shows that the area of the grey region where  $R_H^\infty < 0$  is much larger than that of the black region where  $R_H^\infty > 0$ .

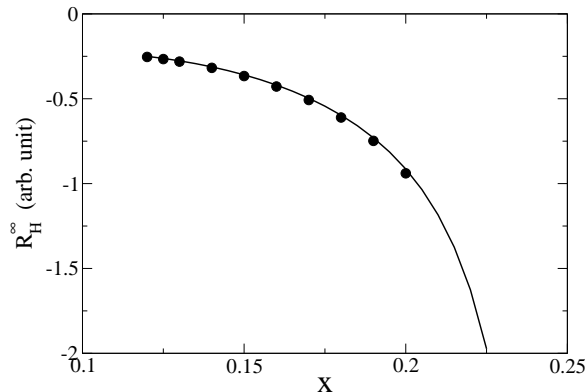


FIG. 12:  $R_H^\infty$  as a function of doping  $x$  for  $V_c = 0$  and the canonical values of the band parameters. Solid line:  $R_H^\infty$  from Eq. [34]. Dots: numerical results for  $V = 10\text{eV}$ .

## B. Coexistence of Charge Stripe Potential and Spin Stripe Potential

In this subsection, we consider the case where  $V_c = \alpha V$  with  $\alpha < 1/2$  and  $V_c \gg t$ . When  $V_c$  is of the same order as  $V$ , the leading order term in the matrix element  $M^A$  is of order  $1/V$ , and it is the only term at this order. To order  $1/V$ , the Hamiltonian in Eq. [8] takes the form

$$H = -2V_c - 2t'' \cos 2p_y - 2t |\cos p_y| + \tilde{f}_1 \cos 4p_x, \quad (35)$$

where

$$\tilde{f}_1 = 2M^A = \frac{2\alpha}{1 - 4\alpha^2} \frac{t''^2}{V}, \quad (36)$$

and terms of order  $1/V$  and independent of  $p_x$  are neglected.

Substituting Eq. [36] into Eq. [11], the Hall conductivity  $\sigma_{xy}$  to leading order in  $1/V$  is

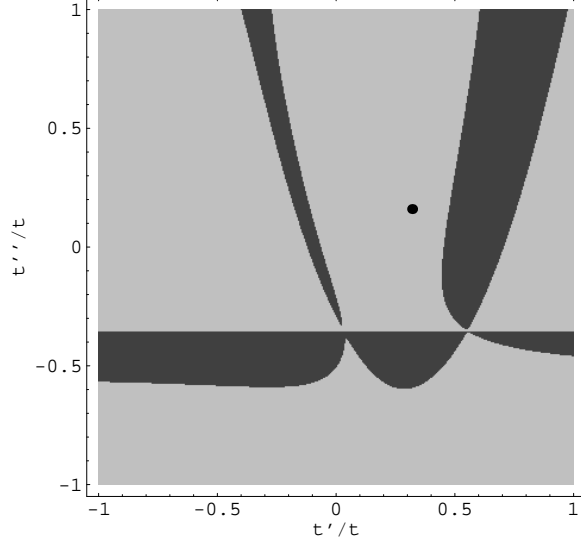


FIG. 13: The sign map of  $R_H^\infty$ , as determined from Eq. [34], for  $V_c = 0$  and doping  $x = 0.125$ . In the dark region  $R_H^\infty > 0$ , and in the grey region  $R_H^\infty < 0$ . The dot represents the point at  $t'/t = 0.32$  and  $t''/t = 0.16$ .

given by

$$\sigma_{xy} = -\frac{16\pi\mathcal{A}m_0}{V^2} \frac{\tilde{f}_1^2}{v_0} \equiv \frac{1}{V^2} \tilde{\mathcal{S}}_{xy}, \quad (37)$$

where we have used  $d\tilde{f}_1/dp_y = 0$ . The longitudinal conductivities  $\sigma_{xx}$  and  $\sigma_{yy}$  are calculated in a similar manner, to leading order in  $1/V$ ,

$$\sigma_{xx} = \frac{1}{V^2} \mathcal{B} \frac{16\pi}{|v_0|} \tilde{f}_1^2 \equiv \frac{1}{V^2} \tilde{\mathcal{S}}_{xx}, \quad (38)$$

and  $\sigma_{yy}$  is given by Eq. [33]. So,  $R_H$  approaches a constant in the  $V \rightarrow \infty$  limit,

$$\lim_{V \rightarrow \infty} R_H \equiv \tilde{R}_H^\infty = \frac{\tilde{\mathcal{S}}_{xy}}{\tilde{\mathcal{S}}_{xx} \sigma_{yy}^\infty} \sim -\frac{m_0}{v_0}. \quad (39)$$

We see that  $\tilde{\mathcal{S}}_{xy}$ ,  $\tilde{\mathcal{S}}_{xx}$ ,  $\sigma_{yy}^\infty$ , and  $\tilde{R}_H^\infty$  are determined by the ratio  $\alpha = V_c/V$ , the hole doping  $x$ , and the band parameters  $t$ ,  $t'$  and  $t''$ . The numerical results of the conductivities  $\sigma_{xx,xy,yy}$  and the Hall coefficient  $R_H$  for the charge stripe potential  $V_c$  up to 50eV, the spin stripe potential  $V = 3V_c$ , doping  $x = 0.125$ , and the canonical values of the band parameters are shown in Fig. [14], where we compare the results to the corresponding  $V \rightarrow \infty$  limits. We observe that the numerical results approach the expected values, with small discrepancies which we attribute to the errors in calculating the chemical potential and in finding the Fermi surface numerically. For the parameters used here,  $\tilde{R}_H^\infty < 0$ .

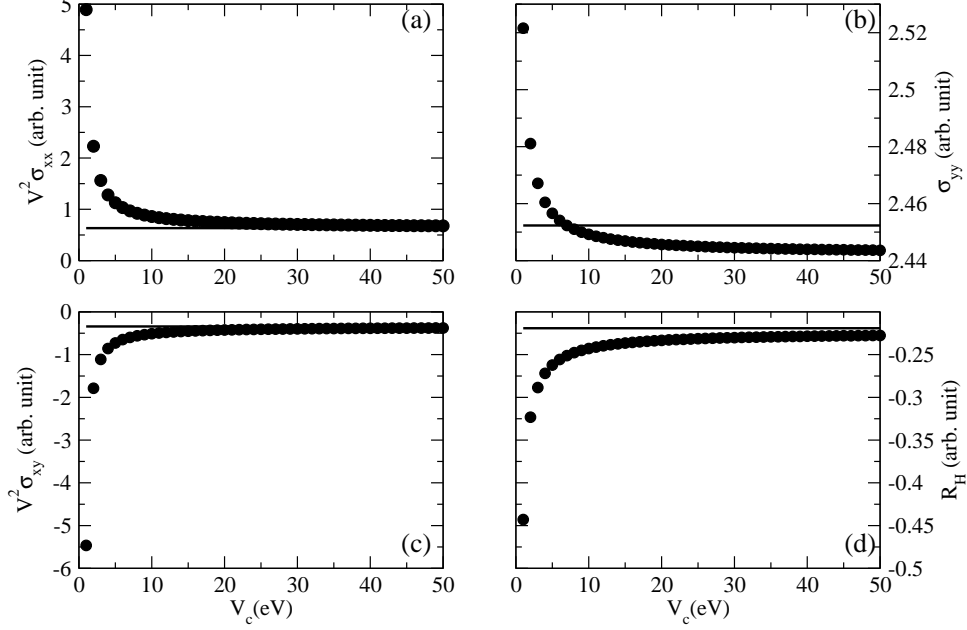


FIG. 14: Transport coefficients in the large spin and charge stripe potentials for  $V = 3V_c$ , doping  $x = 0.125$ , and the canonical values of the band parameters. (a):  $V^2\sigma_{xx}$  (dots) and  $\tilde{\mathcal{S}}_{xx}$  (solid line). (b):  $\sigma_{yy}$  (dots) and  $\sigma_{yy}^\infty$  (solid line). (c):  $V^2\sigma_{xy}$  (dots) and  $\tilde{\mathcal{S}}_{xy}$  (solid line). (d):  $R_H$  (dots) and  $\tilde{R}_H^\infty$  (solid line).

Eq. [39] shows that  $\tilde{R}_H^\infty$  is entirely determined by the curvature of the 1D band at  $p_0$ :  $m_0/v_0$ . We now study  $\tilde{R}_H^\infty$  as a function of doping and the band parameters. In Fig. [15(a)], we plot  $\tilde{R}_H$  as a function of doping  $x$  for the canonical values of the band parameters,  $t'/t = 0.32$  and  $t''/t = 0.16$ . We see that for this set of band parameters,  $\tilde{R}_H^\infty < 0$  for doping  $0.125 < x < 0.25$ , because both  $m_0$  and  $v_0$  are positive in this doping range. In fact, it is easy to see that  $\tilde{R}_H^\infty < 0$  in this doping range as long as  $t''/t > 0$ . Since  $\varepsilon^0(p_y)$  is independent of  $t'$ , we only need to study the effects of  $t''/t$  on  $\tilde{R}_H^\infty$ . Fig. [15(b)] shows  $\tilde{R}_H^\infty$  as a function of  $t''/t$  for the doping  $x = 0.125$ . We see that  $\tilde{R}_H^\infty < 0$  for  $-0.32 < t''/t < 0.32$ .

We mention that when the charge stripe potential  $V_c \sim t$  and  $V_c \ll V$ ,  $\tilde{f}_1$  in Eq. [36] is of the same order as  $f_1$  in Eq. [29] and  $f_2$  in Eq. [30]. In this case, to leading order  $1/V^2$ , the Hamiltonian  $H$  in Eq. [8] has the form of Eq. [28]; the only difference is that the coefficient of  $\cos 4p_x$  is now given by  $f_1 + \tilde{f}_1$ . The Hall effect in this case is then similar to that in the  $V_c = 0$  case.

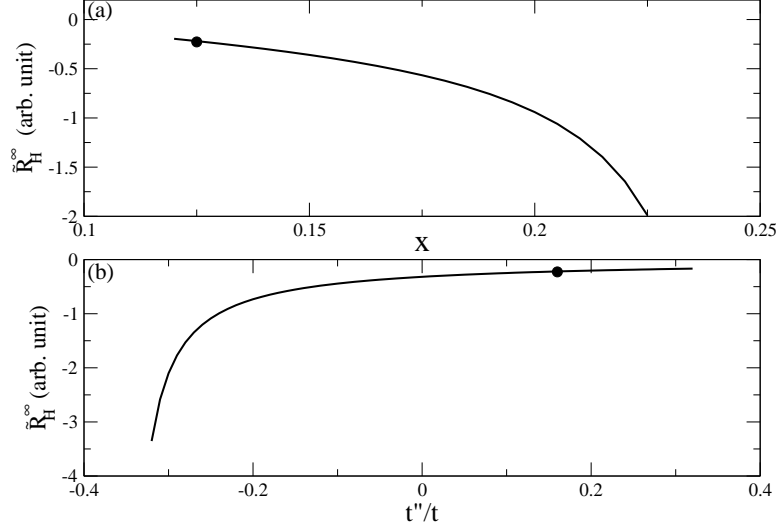


FIG. 15: (a):  $\tilde{R}_H^\infty$  as a function of doping  $x$ , for  $V_c/V = 1/3$  and  $t''/t = 0.16$ . (b):  $\tilde{R}_H^\infty$  as a function of  $t''/t$ , for  $V_c = V/3$  and doping  $x = 0.125$ . In both plots solid lines are results from Eq. [39], and dots are from numerical calculation for  $V_c = 50\text{eV}$ ,  $V = 150\text{eV}$ , doping  $x = 0.125$ ,  $t'/t = 0.32$ , and  $t''/t = 0.16$ .

## VII. DISCUSSION

To conclude, we have considered the Hall effect in a stripe-ordered system. We found that the Hall effect  $R_H$  shows complicated behavior as the spin stripe potential  $V$  and/or the charge stripe potential  $V_c$  are varied. For moderate values of  $V$  and  $V_c$ , the behavior of  $R_H$  can be understood as a result of the change of the Fermi surface topology, which is quite sensitive to the tuning of the stripe order potentials. In the strong coupling limit, the sign of  $R_H$  was also found to depend on details.

In a model with only static spin stripe potential  $V$ ,  $R_H$  first increases from a positive band value  $R_H^0$ , then decreases to negative values, and goes back to positive values, as increasing  $V$  up to  $\sim 1\text{eV}$ , and then has a further sign change at unphysically large  $V$ . This initial increase and the subsequent change of sign qualitatively agrees with the experimental data. This is further supported from the model calculation in which  $V$  is assumed to increase when decreasing doping from  $x = 0.24$ , as shown in Fig. [8]. We mention that analogous calculations (not shown here) based on spiral order, do not produce a sign change. In a model with only static charge stripe potential  $V_c$ , our calculation shows that  $R_H$  increases from the band value until a sign change at  $V_c \approx 0.8\text{eV}$ , after which the sign assumes the

strong coupling limit electron-like value. This is qualitatively inconsistent with experimental data.

When both the static spin stripe potential and the charge stripe potential are present,  $R_H$  can be strongly enhanced or can be made negative by tuning  $V$  and  $V_c$ , as shown in Fig. [7]. While both the spin stripe model and the  $V&V_c$  model produce a sign change in  $R_H$ , the mechanisms are different. In the spin stripe model, the sign change of  $R_H$  is due to the electron pocket centered at  $(0, \pi)$  and the elimination of the hole pockets centered at  $(\pm\pi/8, \pi/2)$ . In the spin and charge stripe model, the sign change is due to the merging of the hole pockets into open Fermi surface and the appearance of the electron pocket centered at  $(0, 0)$ . Measurements directly probing the Fermi surfaces are required to distinguish these two scenarios. In our calculation, we found that the open Fermi surface can give either a positive (*i.e.* hole-like) contribution or a negative (*i.e.* electron-like) contribution to  $\sigma_{xy}$ . Under certain situations, especially when there is only open Fermi surface, this contribution, albeit small, is important, since the small  $\sigma_{xx}$  would compensate the smallness of  $\sigma_{xy}$  to give a large  $|R_H|$ ; the  $V = 0.3\text{eV}$ ,  $V_c = 0$  point in Fig. [5(d)] and the  $V = 0.25\text{eV}$ ,  $V_c = 0.7\text{eV}$  point in Fig. [7(b)] are two examples. However, once there are electron or hole pockets, the contribution to  $\sigma_{xy}$  from the open Fermi surface is negligible, and thus the sign of  $R_H$  is fixed.

We also considered the large stripe potential limit, in which the system is quasi-one dimensional, and the Fermi surface is open. We showed that analytical results of  $R_H$  can be obtained in the limit  $V \gg t$ , both for  $V \gg V_c$  and for  $V > 2V_c \gg t$ . In this limit,  $R_H$  depends on the carrier density, the electron band parameters, and the charge potential  $V_c$ , and its sign can be positive or negative.

There remain discrepancies between experiment and theory. Experiment shows that  $R_H$  at  $x = 0.2$  is about 4 times larger than that at  $x = 0.24$ , while our calculation only shows a factor of 2. However, the magnitude of  $R_H$  depends crucially on the details of the Fermi surface. Angle dependence of the scattering rate<sup>19</sup> (not considered here) may also be important. A systematic study of the doping dependence of the low temperature Hall effect, as was done on PCCO,<sup>10</sup> would be helpful. But, the crucial generic result of our calculation is that the sign change of  $R_H$  observed in Refs. [8,9] appears to be strong evidence in favor of a spin-stripe order.



## Acknowledgments

We thank the authors of Ref. [8] for sharing their data in advance of publication, and M. R. Norman for helpful discussions. This work was supported by NSF–DMR–0705847.

- 
- <sup>1</sup> J. Orenstein and A. J. Millis, *Science* **288**, 468 (2000).
  - <sup>2</sup> S. A. Kivelson, I. P. Bindloss, E. Fradkin, V. Oganesyan, J. M. Tranquada, A. Kapitulnik, and C. Howald, *Rev. Mod. Phys.* **75**, 1201 (2003).
  - <sup>3</sup> A. J. Millis and M. R. Norman, *Phys. Rev. B* **76** 220503(R) (2007).
  - <sup>4</sup> N. Doiron-Leyraud, C. Proust, D. LeBoeuf, J. Levallois, J.-B. Bonnemaïson, R. Liang, D. A. Bonn, W. N. Hardy, and L. Taillefer, *Nature*, **447**, 565 (2007).
  - <sup>5</sup> A. F. Bangura, J. D. Fletcher, A. Carrington, J. Levallois, M. Nardone, B. Vignolle, P. J. Heard, N. Doiron-Leyraud, D. LeBoeuf, L. Taillefer, S. Adachi, C. Proust, and N. E. Hussey, *Phys. Rev. Lett.*, **100**, 047004 (2008).
  - <sup>6</sup> A. R. Moodenbaugh, Y. Xu, M. Suenaga, T. J. Folkerts, and R. N. Shelton, *Phys. Rev. B* **38**, 4596 (1988).
  - <sup>7</sup> N. Ichikawa, S. Uchida, J. M. Tranquada, T. Niemöller, P. M. Gehring, S.-H. Lee, and J. R. Schneider, *Phys. Rev. Lett.* **85**, 1738 (2000).
  - <sup>8</sup> R. Daou, D. LeBoeuf, N. Doiron-Leyraud, S. Y. Li, F. Laliberte, O. Cyr-Choiniere, Y. J. Jo, L. Balicas, J. -Q. Yan, J. -S. Zhou, J. B. Goodenough, L. Taillefer, arXiv.0806.2881 (2008).
  - <sup>9</sup> Y. Nakamura and S. Uchida, *Phys. Rev. B* **46**, 5841 (1992).
  - <sup>10</sup> Y. Dagan, M. M. Qazilbash, C. P. Hill, V. N. Kulkarni, and R. L. Greene, *Phys. Rev. Lett.* **92**, 167001 (2004).
  - <sup>11</sup> Jie Lin and A. J. Millis, *Phys. Rev. B* **72**, 214506 (2005).
  - <sup>12</sup> O. K. Andersen, A. I. Liechtenstein, O. Jepsen and F. Paulsen, *J. Phys. Chem. Solids* **56**, 1573 (1995).
  - <sup>13</sup> J. M. Tranquada, J. D. Axe, N. Ichikawa, A. R. Moodenbaugh, Y. Nakamura, and S. Uchida, *Phys. Rev. Lett.*, **78**, 338 (1997)
  - <sup>14</sup> J. M. Tranquada, B. J. Sternlieb, J. D. Axe, Y. Nakamura, and S. Uchida, *Nature* **375**, 561 (1995).

- <sup>15</sup> O. Zachar, S. A. Kivelson, and V.J. Emery, Phys. Rev. B **57**, 1422 (1998).
- <sup>16</sup> J. Fenton and A. J. Schofield, Phys. Rev. Lett. **95**, 247201 (2005).
- <sup>17</sup> E. I. Blount, Phys. Rev. **126**, 1636 (1962).
- <sup>18</sup> N. P. Ong, Phys. Rev. B **43**, 193 (1991).
- <sup>19</sup> N. E. Hussey, J. Phys. Cond. Mat. **20**, 123201 (2008).